Proceedings of the Reactor Physics Asia 2023 (RPHA2023) Conference
Gyeongju, Korea, October 24-26, 2023

Pin-cell Homogenization for PWR-Core Pin-by-pin P_1 Calculation

Junwei Qin, Yunzhao Li*
Xi'an Jiaotong University, 28 West Xianning Road, Xi'an, Shaanxi 710049, P.R. China
**Yunzhao Li: yunzhao@mail.xjtu.edu.cn*

1. Introduction

With the development of advanced nuclear reactor, the heterogeneity and neutron leakage of the Pressurized Water Reactor (PWR) core is becoming stronger and stronger. Under this circumstance, the traditional two-step method based on assembly homogenization cannot meet the requirements of the engineering calculation accuracy. Therefore, the pin-by-pin calculation based on pin-cell homogenization has gradually become an important option as the next-generation routine calculation approach.

Most of the pin-by-pin calculation programs introduce diffusion or SP_3 approximation in the neutronics calculation, such as NECP-Bamboo2.0[1], SCOPE2[2], SPHINCS[3] and so on. However, for the whole-core Pin-by-pin SP_3 calculation, its spatial grid can reach tens of millions of orders of magnitude, with at least 4 or even 7 energy groups. The computational cost, including both storage requirements and computing time, still needs to be further reduced.

In the three-dimensional whole-core pin-by-pin calculation, the SP_3 neutronics calculation spends the largest portion of the computational effort. Therefore, the P_1 approximation, which shares the same form with the neutron diffusion equation, is expected to half the calculation cost. Compared with diffusion approximation, the P_1 approximation can also remove the transport correction by retaining the first-order anisotropic scattering source. Therefore, this paper concentrates on the pin-cell homogenization for PWR-core pin-by-pin P_1 calculation.

2. Theoretical Models

2.1 The P_1 Equation

The multi-group steady-state neutron transport equation is shown below:

$$\begin{aligned}&\boldsymbol{\Omega}\cdot\nabla\varphi_g(\boldsymbol{r},\boldsymbol{\Omega})+\Sigma_{\mathrm{t},g}(\boldsymbol{r})\varphi_g(\boldsymbol{r},\boldsymbol{\Omega})\\&=\sum_{g'=1}^{G}\int_{4\pi}\Sigma_{\mathrm{s},g'\to g}(\boldsymbol{r},\boldsymbol{\Omega}'\to\boldsymbol{\Omega})\varphi_g(\boldsymbol{r},\boldsymbol{\Omega}')\mathrm{d}\boldsymbol{\Omega}'\\&+\frac{1}{k_{\mathrm{eff}}}\frac{\chi_g(\boldsymbol{r})}{4\pi}\sum_{g'=1}^{G}\int_{4\pi}\nu\Sigma_{\mathrm{f},g'}(\boldsymbol{r})\varphi_{g'}(\boldsymbol{r},\boldsymbol{\Omega}')d\boldsymbol{\Omega}'\end{aligned}\tag{1}$$

where $\boldsymbol{r}$ is the spatial location, φ_g is the neutron angular flux of group g ($cm^{-2}\cdot s^{-1}$), $\boldsymbol{\Omega}$ is the neutron motion direction, $\Sigma_{\mathrm{t},g}$ and $\Sigma_{\mathrm{f},g}$ are respectively the total and fission cross-sections of group g (cm^{-1}), $\Sigma_{\mathrm{s},g'\to g}$ is the scattering cross-section from group g' to group g (cm^{-1}), χ_g is the neutron fission spectrum of group g, ν is the number of neutrons per fission, g=1, 2, …, G is the neutron energy group index.

Based on the first-order expansion of angular flux and scattering cross-section in terms of angular, the P_1 equation can be obtained:

$$\nabla\boldsymbol{J}_g(\boldsymbol{r})+\Sigma_{\mathrm{t},g}\phi_g(\boldsymbol{r})=\sum_{g'=1}^{G}\Sigma_{\mathrm{s0},gg'}\phi_{g'}(\boldsymbol{r})+\frac{\chi_g}{k_{\mathrm{eff}}}\sum_{g=1}^{G}\nu\Sigma_{\mathrm{f},g'}\phi_{g'}(\boldsymbol{r})\tag{2}$$

$$\frac{1}{3}\nabla\phi_g(\boldsymbol{r})+\Sigma_{\mathrm{t},g}\boldsymbol{J}_g(\boldsymbol{r})=\sum_{g'=1}^{G}\Sigma_{\mathrm{s1},gg'}\boldsymbol{J}_{g'}(\boldsymbol{r})\tag{3}$$

where, ϕ_g is the neutron scalar flux of group g ($cm^{-2}\cdot s^{-1}$), J_g is the neutron current of group g ($cm^{-2}\cdot s^{-1}$), $\Sigma_{\mathrm{s1},g'\to g}$ is the first-order anisotropic scattering cross-section from group g' to group g (cm^{-1}).

Defining the diffusion coefficient matrix as:

$$\overline{\overline{D}}=\frac{1}{3}\left(\overline{\overline{\Sigma}}_{\mathrm{t}}-\overline{\overline{\Sigma}}_{\mathrm{s1}}\right)^{-1}\tag{4}$$

can transfer the P_1 Eq. into:

$$-\nabla\overline{\overline{D}}\,\nabla\boldsymbol{\phi}(\boldsymbol{r})+\overline{\overline{\Sigma}}_{\mathrm{t}}\boldsymbol{\phi}(\boldsymbol{r})=\boldsymbol{S}\tag{5}$$

where,

$$S_g=\sum_{g'=1}^{G}\Sigma_{\mathrm{s0},gg'}\phi_{g'}(\boldsymbol{r})+\frac{\chi_g}{k_{\mathrm{eff}}}\sum_{g'=1}^{G}\nu\Sigma_{\mathrm{f},g'}\phi_{g'}(\boldsymbol{r})\tag{6}$$

Eq. (5) is formally identical to the diffusion equation, so the computational efficiency is theoretically the same as the diffusion equation. Meanwhile, due to retaining the first-order anisotropic scattering source and no longer introducing transport correction, the calculation accuracy should be higher than the diffusion equation.

2.2 Finite Difference Solution of the P_1 Equation

Eq. (5) can be discretized by using the finite difference method in three-dimensional Cartesian coordinates:

$$\begin{aligned}&-\frac{\partial}{\partial x}[\overline{\overline{D}}(\mathrm{x,y,z})\frac{\partial}{\partial x}\phi(\mathrm{x,y,z})]-\frac{\partial}{\partial y}[\overline{\overline{D}}(\mathrm{x,y,z})\frac{\partial}{\partial y}\phi(\mathrm{x,y,z})]\\&-\frac{\partial}{\partial z}[\overline{\overline{D}}(\mathrm{x,y,z})\frac{\partial}{\partial z}\phi(\mathrm{x,y,z})]+\overline{\overline{\Sigma}}_{\mathrm{t}}\phi(\mathrm{x,y,z})=\overline{\overline{S}}(x,y,z)\end{aligned}\tag{7}$$

Defining the flux at the center of the mesh (x_i,y_j,z_k) as $\phi_{i,j,k}$ and integrating Eq. (7) in the mesh lead to:

$$\begin{aligned}&\iiint\{-\frac{\partial}{\partial x}[\overline{\overline{D}}(\mathrm{x,y,z})\frac{\partial}{\partial x}\phi(\mathrm{x,y,z})]-\frac{\partial}{\partial y}[\overline{\overline{D}}(\mathrm{x,y,z})\frac{\partial}{\partial y}\phi(\mathrm{x,y,z})]\\&-\frac{\partial}{\partial z}[\overline{\overline{D}}(\mathrm{x,y,z})\frac{\partial}{\partial z}\phi(\mathrm{x,y,z})]\}dxdydz\\&+\iiint\overline{\overline{\Sigma}}_{\mathrm{t}}\phi(\mathrm{x,y,z})dxdydz=\iiint S(x,y,z)dxdydz\end{aligned}\tag{8}$$

Define the leakage of u-direction as L_u:

$$L_u=\frac{2}{\Delta u_i}\frac{\overline{\overline{D}}_u}{\Delta u_i}[-\phi_i^{u^-}+2\phi_i-\phi_i^{u^+}]\tag{9}$$

By solving the surface flux and substituting it into Eq. (9), the discretized P_1 equation can be obtained:

$$\sum_{u}^{u=x,y,z}\frac{2}{\Delta u}\left[\overline{\overline{A}}\phi_{i-1}+\overline{\overline{B}}\phi_i+\overline{\overline{C}}\phi_{i+1}\right]+\overline{\overline{\Sigma}}_{\mathrm{t},i,j,k}\phi_{i,j,k}=\overline{s}_{i,j,k}\tag{10}$$

where,

$$\overline{\overline{A}} = -\frac{\overline{\overline{D}}_u}{\Delta u_i}\left(\frac{\overline{\overline{D}}_u}{\Delta u_i}+\frac{f_i^{u^-}}{f_{i-1}^{u^+}}\frac{\overline{\overline{D}}_{u-1}}{\Delta u_{i-1}}\right)^{-1}\frac{\overline{\overline{D}}_{u-1}}{\Delta u_{i-1}} \tag{11}$$

$$\overline{\overline{B}} = 2\frac{\overline{\overline{D}}_u}{\Delta u_i}-\frac{\overline{\overline{D}}_u}{\Delta u_i}\left(\frac{\overline{\overline{D}}_u}{\Delta u_i}+\frac{f_i^{u^-}}{f_{i-1}^{u^+}}\frac{\overline{\overline{D}}_{u-1}}{\Delta u_{i-1}}\right)^{-1}\frac{\overline{\overline{D}}_u}{\Delta u_i} -\frac{\overline{\overline{D}}_u}{\Delta u_i}\left(\frac{\overline{\overline{D}}_u}{\Delta u_i}+\frac{f_i^{u^+}}{f_{i+1}^{u^-}}\frac{\overline{\overline{D}}_{u+1}}{\Delta u_{i+1}}\right)^{-1}\frac{\overline{\overline{D}}_u}{\Delta u_i} \tag{12}$$

$$\overline{\overline{C}} = -\frac{\overline{\overline{D}}_u}{\Delta u_i}\left(\frac{\overline{\overline{D}}_u}{\Delta u_i}+\frac{f_i^{u^+}}{f_{i+1}^{u^-}}\frac{\overline{\overline{D}}_u}{\Delta u_i}\right)^{-1}\frac{\overline{\overline{D}}_{u+1}}{\Delta u_{i+1}} \tag{13}$$

Compared with the traditional diffusion equation, the energy group of the P_1 equation cannot be decoupled due to the coupling in the diffusion coefficient matrix. Thus, the following iterative solution flow was employed:

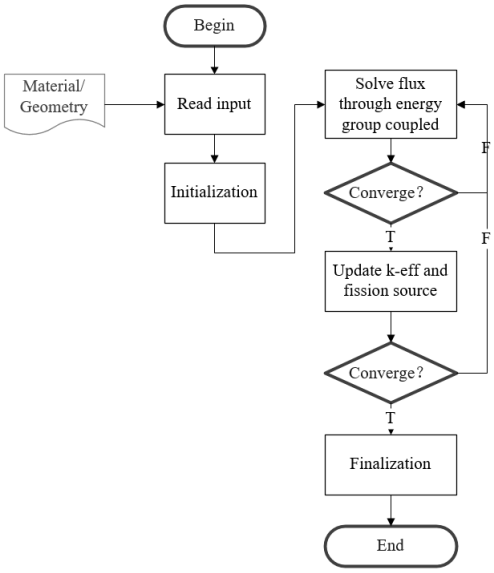

Fig. 1. Iterative flowchart of P_1 equation.

2.3 Pin-cell Homogenization for P_1 calculation

During the homogenization, the following quantities are required to be conserved:

1) The effective multiplication coefficient:

$$k_{\text{eff}}^{\text{het}} = k_{\text{eff}}^{\text{hom}} \tag{14}$$

2) The scalar reaction rates in each homogenization region:

$$\int_V\int_{4\pi}\boldsymbol{\Omega}\cdot\nabla\varphi_g^{\text{het}}(\boldsymbol{r},\boldsymbol{\Omega})\,\mathrm{d}\boldsymbol{\Omega}\mathrm{d}v=\int_V\nabla\boldsymbol{J}_g^{\text{hom}}(\boldsymbol{r})\,\mathrm{d}v \tag{15}$$

$$\int_V\int_{4\pi}\Sigma_{\text{t},g}^{\text{het}}(\boldsymbol{r})\varphi_g^{\text{het}}(\boldsymbol{r},\boldsymbol{\Omega})\,\mathrm{d}\boldsymbol{\Omega}\mathrm{d}v=\int_V\Sigma_{\text{t},g}^{\text{hom}}\phi_g^{\text{hom}}(\boldsymbol{r})\,\mathrm{d}v \tag{16}$$

$$\int_V\int_{4\pi}\int_{4\pi}\Sigma_{\text{s},g'\to g}(\boldsymbol{r},\boldsymbol{\Omega}'\to\boldsymbol{\Omega})\varphi_{g'}^{\text{het}}(\boldsymbol{r},\boldsymbol{\Omega}')\,\mathrm{d}\boldsymbol{\Omega}'\mathrm{d}\boldsymbol{\Omega}\mathrm{d}v =\int_V\Sigma_{\text{s0},gg'}^{\text{hom}}\phi_{g'}^{\text{hom}}(\boldsymbol{r})\mathrm{d}v \tag{17}$$

$$\int_V\int_{4\pi}\int_{4\pi}\frac{\chi_g(\boldsymbol{r})}{4\pi}\nu\Sigma_{\text{f},g'}(\boldsymbol{r})\varphi_{g'}^{\text{het}}(\boldsymbol{r},\boldsymbol{\Omega}')\,\mathrm{d}\boldsymbol{\Omega}'\mathrm{d}\boldsymbol{\Omega}\mathrm{d}v =\int_V\chi_g^{\text{hom}}\nu\Sigma_{\text{f},g'}^{\text{hom}}\phi_{g'}^{\text{hom}}(\boldsymbol{r})\,\mathrm{d}v \tag{18}$$

3) The scalar neutron leakage rate on each surface in the x/y/z directions:

$$\int_V\int_{4\pi}\Omega_u\boldsymbol{\Omega}\cdot\nabla\varphi_g^{\text{het}}(\boldsymbol{r},\boldsymbol{\Omega})\,\mathrm{d}\boldsymbol{\Omega}\mathrm{d}v=\int_V\frac{1}{3}\nabla_u\phi_g^{\text{hom}}(\boldsymbol{r})\mathrm{d}v \tag{19}$$

$$\int_V\int_{4\pi}\Omega_u\Sigma_{\text{t},g}^{\text{het}}(\boldsymbol{r})\varphi_g^{\text{het}}(\boldsymbol{r},\boldsymbol{\Omega})\,\mathrm{d}\boldsymbol{\Omega}\mathrm{d}v=\int_V\Sigma_{\text{t},g}^{\text{hom}}J_{u,g}^{\text{hom}}(\boldsymbol{r})\mathrm{d}v \tag{20}$$

$$\int_V\int_{4\pi}\int_{4\pi}\Omega_u\Sigma_{\text{s},g'\to g}(\boldsymbol{r},\boldsymbol{\Omega}'\to\boldsymbol{\Omega})\varphi_g^{\text{het}}(\boldsymbol{r},\boldsymbol{\Omega}')\,\mathrm{d}\boldsymbol{\Omega}'\mathrm{d}\boldsymbol{\Omega}\mathrm{d}v =\int_V\Sigma_{\text{s1},gg'}^{\text{hom}}J_{u,g'}^{\text{hom}}(\boldsymbol{r})\mathrm{d}v \tag{21}$$

$$\int_V\int_{4\pi}\Omega_u\frac{\chi_g(\boldsymbol{r})}{4\pi}\int_{4\pi}\nu\Sigma_{\text{f},g'}(\boldsymbol{r})\varphi_{g'}^{\text{het}}(\boldsymbol{r},\boldsymbol{\Omega}')\,\mathrm{d}\boldsymbol{\Omega}'\mathrm{d}\boldsymbol{\Omega}\mathrm{d}v=0 \tag{22}$$

Meanwhile, considering the neutron flux density and the neutron current density in the homogenization region also need to be conserved:

$$\int_V\int_{4\pi}\varphi_g^{\text{het}}(\boldsymbol{r},\boldsymbol{\Omega})\,\mathrm{d}\boldsymbol{\Omega}\mathrm{d}v=\int_V\phi_g^{\text{hom}}(\boldsymbol{r})\,\mathrm{d}v \tag{23}$$

$$\int_V\int_{4\pi}\Omega_u\varphi_g^{\text{het}}(\boldsymbol{r},\boldsymbol{\Omega})\,\mathrm{d}\boldsymbol{\Omega}\mathrm{d}v=\int_V J_{u,g}^{\text{hom}}(\boldsymbol{r})\mathrm{d}v \tag{24}$$

The diffusion coefficient matrix can be obtained according to Eq. (4), in which the total and first-order scattering matrices can be obtained as:

$$\overline{\overline{\Sigma}}_{\text{t}}^{\text{hom}} = \begin{bmatrix} \Sigma_{\text{t},x,1}^{\text{hom}} & & & & & & \\ & \ddots & & & & & \\ & & \Sigma_{\text{t},x,g}^{\text{hom}} & & & & \\ & & & \ddots & & & \\ & & & & \Sigma_{\text{t},x,G}^{\text{hom}} & & \\ & & & & & \Sigma_{\text{t},z,1}^{\text{hom}} & \\ & & & & & & \ddots \\ & & & & & & & \Sigma_{\text{t},z,G}^{\text{hom}} \end{bmatrix} \tag{25}$$

$$\overline{\overline{\Sigma}}_{\text{s1}}^{\text{hom}} = \begin{bmatrix} \Sigma_{\text{s1},x,11}^{\text{hom}} & \cdots & \Sigma_{\text{s1},x,1g}^{\text{hom}} & \cdots & \Sigma_{\text{s1},x,1G}^{\text{hom}} & & & & \\ \vdots & & \vdots & & \vdots & & & & \\ \Sigma_{\text{s1},x,g1}^{\text{hom}} & \cdots & \Sigma_{\text{s1},x,gg}^{\text{hom}} & \cdots & \Sigma_{\text{s1},x,gG}^{\text{hom}} & & & & \\ \vdots & & \vdots & & \vdots & & & & \\ \Sigma_{\text{s1},x,G1}^{\text{hom}} & \cdots & \Sigma_{\text{s1},x,Gg}^{\text{hom}} & \cdots & \Sigma_{\text{s1},x,GG}^{\text{hom}} & & & & \\ & & & & & \Sigma_{\text{s1},z,11}^{\text{hom}} & \cdots & \Sigma_{\text{s1},z,1g}^{\text{hom}} & \cdots & \Sigma_{\text{s1},z,1G}^{\text{hom}} \\ & & & & & \vdots & & \vdots & & \vdots \\ & & & & & \Sigma_{\text{s1},z,g1}^{\text{hom}} & \cdots & \Sigma_{\text{s1},z,gg}^{\text{hom}} & \cdots & \Sigma_{\text{s1},z,gG}^{\text{hom}} \\ & & & & & \vdots & & \vdots & & \vdots \\ & & & & & \Sigma_{\text{s1},z,G1}^{\text{hom}} & \cdots & \Sigma_{\text{s1},z,Gg}^{\text{hom}} & \cdots & \Sigma_{\text{s1},z,GG}^{\text{hom}} \end{bmatrix} \tag{26}$$

According to the Gauss Law, the total leakage of the homogenization region boundary can be written as:

$$\int_\Gamma\int_{4\pi}\langle\boldsymbol{n}_s,\boldsymbol{\Omega}\rangle\boldsymbol{\varphi}^{\text{het}}(\boldsymbol{r},\boldsymbol{\Omega})\,\mathrm{d}\boldsymbol{\Omega}\mathrm{d}s=\int_\Gamma\left\langle\boldsymbol{n}_s,-\overline{\overline{D}}^{\text{hom}}\nabla\boldsymbol{\phi}^{\text{hom}}(\boldsymbol{r})\right\rangle\mathrm{d}s \tag{27}$$

On each surface, it can become:

$$\int_{\Gamma_i}\int_{4\pi}\langle\boldsymbol{n}_s,\boldsymbol{\Omega}\rangle\boldsymbol{\varphi}^{\text{het}}(\boldsymbol{r},\boldsymbol{\Omega})\,\mathrm{d}\boldsymbol{\Omega}\mathrm{d}s=\int_{\Gamma_i}\left\langle\boldsymbol{n}_s,-\overline{\overline{D}}^{\text{hom}}\nabla\boldsymbol{\phi}^{\text{hom}}(\boldsymbol{r})\right\rangle\mathrm{d}s \tag{28}$$

According to the FDM solution of P_1 Eq. in 2.2, the neutron leakage rate after homogenization can be estimated as:

$$\int_{\Gamma_i}\left\langle\boldsymbol{n}_s,-\overline{\overline{D}}^{\text{hom}}\nabla\boldsymbol{\phi}^{\text{hom}}(\boldsymbol{r})\right\rangle\mathrm{d}s=\left\langle\boldsymbol{n}_s,-\overline{\overline{D}}^{\text{hom}}\int_{\Gamma_i}\nabla\boldsymbol{\phi}^{\text{hom}}(\boldsymbol{r})\mathrm{d}s\right\rangle =\overline{\overline{D}}^{\text{hom}}A_{\perp s}\frac{\boldsymbol{\phi}^{\text{hom,Vol}}-\boldsymbol{\phi}^{\text{hom,Sur}}}{\Delta h_s/2} \tag{29}$$

Thus, the estimated homogenized neutron surface flux can be obtained. Therefore, in order to ensure the conservation of the leakage, the discontinuity factors of neutron flux density at the boundary is introduced:

$$f_{i,g}=\frac{\phi_{i,g}^{\text{het,Sur}}}{\phi_{i,g}^{\text{hom,Sur}}} \tag{30}$$

3. Numerical Results

Based on the above methodology, a three-dimensional

solver for P_1 equation has been developed. Correspondingly, a cross-sections homogenization program has also been developed based on the PWR-core pin-by-pin analysis code NECP-Bamboo2.0. In order to verify the effectiveness, numerical results are introduced in this session by taking the one-step heterogeneous calculation results provided by Bamboo-Lattice [4] as the reference. The reason for using the Bamboo-Lattice as the reference is firstly that it is a deterministic one-step program, which provides more accurate calculation results. At the same time, it is the program for generating homogenization constants, which can avoid deviations caused by databases and computational models.

3.1 Single-Assembly Case

A single fuel assembly case is designed, whose diagram is shown in Fig. 2. The reference solution is obtained by Bamboo-Lattice with P_2 scattering. For comparison, in addition to using P_1 approximation for calculation, this paper also uses diffusion approximation and SP_3 approximation calculated by the Exponential Function Expansion Nodal method (EFEN) [5, 6]. The homogenized area is based on the pin-scale. Therefore, in order to ensure the consistency in the calculation area before and after homogenization, all the calculated meshes of the various homogenized calculation method are pin-scale.

As shown in Table I, all k_{eff} obtained by different homogenized calculation are in good agreement with the reference, with the deviations less than 50 pcm. As for the distribution quantities, the bias of the fission rates are shown in Table II and Fig. 3. It can be found that the bias of diffusion approximation is the largest (max 1.39% and the root mean square 0.60%). In contrast, the bias for P_1 and the SP_3 are very close, 0.69% for the max while 0.30% for the RMS. Overall, the deviations of all three methods are acceptable for this example, none of which exceed 1.5%.

According to the traditional homogenization theory, the calculation results should be consistent when the boundary conditions are the same. For this case, due to the reference using P_2 scattering for calculation, and none of three methods can consider such high-order scattering, resulting in a certain deviation.

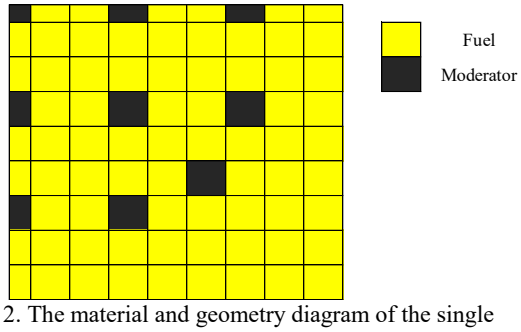

Fig. 2. The material and geometry diagram of the single assembly case.

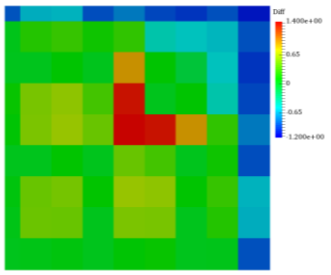

(a) Diffusion approximation

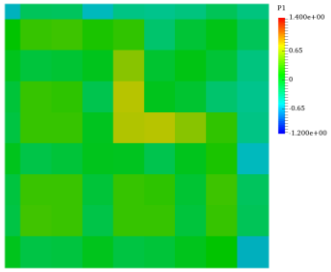

(b) P_1 approximation

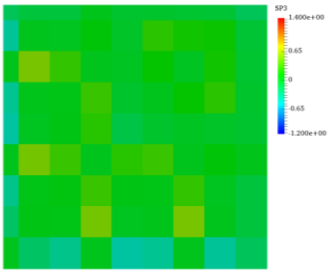

(c) SP_3 approximation

Fig. 3. The bias of fission rate distributions.

Table I: k_{eff} of various methods

	Ref.	Diff.	P_1	SP_3
k_{eff}	1.22925	1.22974	1.22894	1.22942
Bias/pcm	-	49	-31	17

Table II: The bias of fission rates

	Diff.	P_1	SP_3
MAX/%	1.39	0.69	0.50
RMS/%	0.60	0.30	0.22

3.2 Multi-Assemblies Case

For the further verification, a multi-assembly case diagram is shown in Fig. 4. The k_{eff} results are shown in Table III. All k_{eff} results obtained by different homogenized calculation are in good agreement with the reference, with the deviations not exceeding 150 pcm. Among them, the bias of the diffusion approximation is the largest, and the bias of P_1 and SP_3 approximation are very close.

Meanwhile, in order to compare the distribution, this paper compared the bias between the fission rates of different methods and the reference, as shown in Table IV and Fig. 5. For different methods, the bias of the diffusion approximation is the largest, whose max bias is 9.39% and the root mean square bias is 3.98%. In

addition, the P_1 and the SP_3 approximation are very close, both have comparable accuracy. From the Fig. 5, only at the interfaces of the assembly, the bias will be relatively high, and the bias inside the assembly will be minimal, not exceeding 1% for the P_1 and the SP_3 approximation. However, there may also be significant bias inside the assembly for the diffusion approximation.

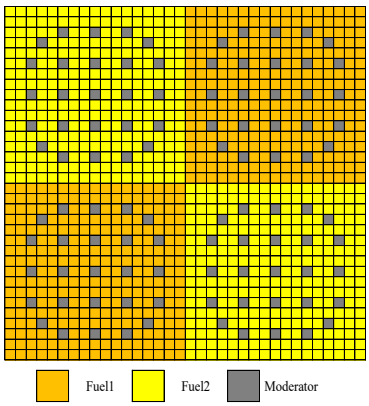

Fig. 4. The diagram of the multi-assembly case.

Table III: The k_{eff} results of various methods

	Ref.	Diff.	P_1	SP_3
k_{eff}	1.08011	1.08123	1.07937	1.08078
Bias/pcm	-	112	-74	67

Table IV: The bias of fission rates

	Diff.	P_1	SP_3
MAX/%	9.39	3.48	4.26
RMS/%	3.98	0.92	0.88

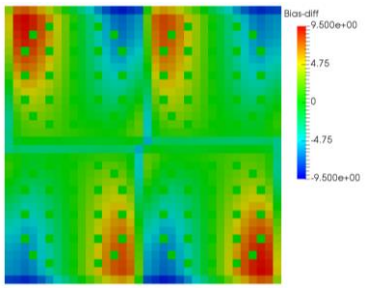

(a) Diffusion approximation

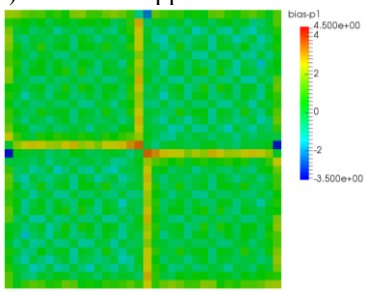

(b) P_1 approximation

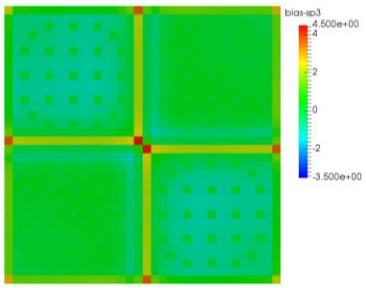

(c) SP_3 approximation

Fig. 5. The bias of fission rate distributions for different method compared with the reference.

4. Conclusions

In order to further improve the efficiency of PWR-core pin-by-pin calculation, this paper proposes a new homogenization and numerical calculation method based on the P_1 equation.

Numerical results indicate that the method has higher accuracy compared to diffusion approximation and is comparable in accuracy to SP_3 approximation. For single assembly case, P_1 method can reduce the deviation to less than 1%. For multi-assemblies case, the deviations of the P_1 method is significantly lower than the diffusion approximation, and this method can reduce the deviation from nearly 10% to 3.5%. Therefore, the new method provides a theoretical basis for the whole-core pin-by-pin calculation, which is expected have practical applications in the future.

The P_1 equation solved in this paper only have one equation, which theoretically has a higher computational efficiency than the two coupled equations of SP_3 approximation.

REFERENCES

[1] Yunzhao Li, et al. "Design and Verification of a PWR-Core Pin-by-Pin Fuel Management Calculation Code." Nuclear Power Engineering 39.S2(2018): 29-32.

[2] Tatsumi Masahiro, and A. Yamamoto. "SCOPE2: Object-Oriented Parallel Code for Multi-group Diffusion/Transport Calculations in Three-Dimensional Fine-mesh Reactor Core Geometry." PHYSOR 2002, ANS Reactor Physics Topical Meeting. Seoul, Korea, October 7-10, 2002.

[3] Hyun Ho Cho, et al. "Preliminary Development of Simplified P_3 based Pin-by-pin Core Simulator, SPHINCS" Transactions of the Korean Nuclear Society Spring Meeting. Jeju, Korea, May 23-24, 2019.

[4] Yunzhao Li, et al. "Development and verification of PWR-core fuel management calculation code system NECP-Bamboo: Part I Bamboo-Lattice." Nuclear Engineering and Design 335.AUG.(2018):432-440.

[5] Tatsumi Masahiro, and A. Yamamoto. "Advanced PWR Core Calculation Based on Multi-group Nodal-transport Method in Three-dimensional Pin-by-Pin Geometry." Journal of Nuclear Science and Technology 40.6(2003):376-387.

[6] Wen Yang, et al. "Acceleration of the exponential function expansion nodal SP3 method by multi-group GMRES algorithm for PWR pin-by-pin calculation." Annals of Nuclear Energy 120.oct.(2018):869-879.